AIAA 97-1018

Heat Transfer Measurements on Surfaces with Natural Ice Castings and Modeled Roughness

K.S. Breuer, B.E. Torres, D.J. Orr and R.J. Hansman
M.I.T.
Cambridge, MA

35th Aerospace Sciences Meeting & Exhibit

January 6-10, 1997 / Reno, NV

Heat Transfer Measurements on Surfaces with Natural Ice Castings and Modeled Roughness

KENNETH S. BREUER*, BENJAMIN E. TORRES†, D. J. ORR†& R. JOHN. HANSMAN‡

Department of Aeronautics and Astronautics
Massachusetts Institute of Technology
Cambridge, MA 02139

Abstract

An experimental method is described to measure and compare the convective heat transfer coefficient of natural and simulated ice accretion roughness and to provide a rational means for determining accretion-related enhanced heat transfer coefficients. The natural ice accretion roughness was a sample casting made from accretions at the NASA Lewis Icing Research Tunnel (IRT). One of these castings was modeled using a Spectral Estimation Technique (SET) to produce three roughness elements patterns that simulate the actual accretion. All four samples were tested in a flat-plate boundary layer at angle of attack in a "dry" wind tunnel test. The convective heat transfer coefficient was measured using infrared thermography. It is shown that, dispite some problems in the current data set, the method does show considerable promise in determining roughness-induced heat transfer coefficients, and that, in addition to the roughness height and spacing in the flow direction, the concentration and spacing of elements in the spanwise direction are important parameters.

Introduction

Computer code simulations, such as NASA's LEWICE, have difficulty matching observed wind tunnel and airplane test results for ice accretions under glaze ice conditions [6]. This mismatch is due in part to an inappropriate heat transfer and boundary layer transition model in which the ice accretion is determined by a heat balance between convective heat transfer at the surface and the release of latent heat of fusion as the water droplets freeze [6].

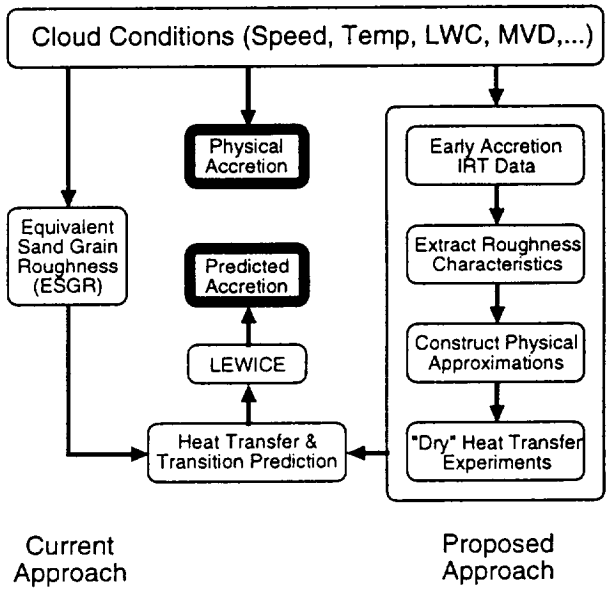

Figure 1: Schematic of current and proposed heat transfer model in LEWICE. Figure reproduced from Orr et al. [12].

The state of the boundary layer influences the heat transfer process since a turbulent boundary layer has a higher convective heat transfer than a laminar boundary layer. The initial ice roughness influences the state of the laminar boundary layer since the initial ice roughness can cause transition from a laminar to a turbulent boundary layer [1, 1, 3]. Thus, the initial ice roughness is very important in the ice accretion process both determining the heat transfer process, the boundary layer transition and the resultant vehicle aerodynamics.

The effect of ice accretion roughness on heat transfer and boundary layer transition is modeled in LEWICE as shown schematically in Figure 1. Currently, the effect of the ice accretion roughness is modeled using the Equivalent Sand Grain Roughness (ESGR) model, as shown on the left side of

*Associate Professor, Member AIAA
†Research Associate
‡Professor, Member AIAA

Figure 1.1. The ESGR model characterizes the ice accretion roughness with a single parameter k. A Reynolds number based on k, Re_k, is used to determine boundary layer transition. Once transition occurs, turbulent heat transfer equations are used with k as a parameter. When glaze ice shape predictions are performed, k is typically adjusted until the experimentally observed shape is obtained. The value of k needed to produce the observed ice shape often bears little significance to the roughness scales observed. Thus, k has little physical meaning, as could be expected since the complicated effect of the ice accretion roughness on the heat transfer and boundary layer transition can not be modeled with a single parameter.

An alternative heat transfer modeling approach based on the micro-physics of the ice accretion process has been proposed [12], and is shown schematically on the right of Figure 1. This heat transfer model incorporates data gathered during icing experiments at the IRT [6, 14]. These experiments have provided high-magnification, close-up video images of the accretion process spanning from the first seconds of the accretion until the final ice shape is established approximately 10 minutes later [6]. Image processing techniques have been used to extract from these video images roughness characteristics corresponding to different cloud conditions. These roughness characteristics can be used to construct physical approximations to the early ice accretion roughness in order to do "dry" wind tunnel tests, concentrating on the effect of the roughness on the convective heat transfer at the surface. In this manner, a heat transfer model based on the micro-physics of the ice accretion process can be developed, providing an alternative to the ESGR model. Pieces of the approach have already been demonstrated. Henry, et al. [7] studied the variation in convective heat transfer coefficients on hemispherical roughness elements mounted on a flat plate in a "dry" wind tunnel using a non-invasive Infra Red (IR) temperature measurement technique. Plastic hemispherical roughness elements, on the order of 2-6mm diameter, and element arrays were studied. Relative convective heat transfer coefficients were calculated showing heat transfer enhancement on the roughness elements. Henry observed significant enhancement in heat transfer on single roughness elements when the elements protruded out of the boundary layer, or when the ratio of roughness height to boundary layer thickness (k/d) was greater than 1.

One of the hardest parts of this model is the method used to reproduce roughness observed in icing tests in a dry heat transfer test. Masiulaniec et al. used direct castings of long-time roughness growths and studied the convective heat transfer coefficient of natural ice accretion aluminum castings on a flat plate in a "dry" wind tunnel [5, 10]. However, these castings were from accretions that had run several minutes and thus are not directly applicable to the early accretion heat transfer problem. Orr et al. [11, 12] took a different approach in which they studied high-magnification video data of Hansman et al [6] which documented early accretions on and near the leading edge of a four inch cylinder. Using a signal processing technique they named SET, Orr et al. identified a small number of geometric parameters that were thought to represent the icing. In the cases examined, average roughness element size and spacing in both the streamwise and spanwise directions were extracted. Using these parameters, they created artificial roughness with the same SET description by depositing small beads of epoxy on plexiglass substrates. This technique, however, has a degree of arbitrariness in the way in which the beads are deposited. Orr et al. showed three possible varients: a rectangular array of regularly spaced beads, an array of regularly spaced beads with each line offset by some amount, and a "pseduo-random" array in which the beads are placed according to a random algorithm such that the resultant array does not have a regular repeating pattern but nevertheless does adhere to the proscribed SET parameters. The samples created by this technique are ideal for dry wind tunnel heat transfer tests (that, indeed was the motivation behind Orr et al.'s work), and the current paper uses Orr's roughness elements for dry testing.

The objective of this experiment is to take each of the pieces of this new proposed model for ice-enhanced heat transfer (Figure 1) and to link them together into a rational and traceble method for providing boundary layer heat transfer coefficients in icing codes such as LEWICE. To accomplish this, we utilize the roughness model derived from the direct castings of Masiulaniec, as well as roughness samples created from the SET analysis of the castings, created using the bead-placement technoque developed by Orr et al. [12]. One question to be answered is whether the SET parameters selected by Orr et al [12] (roughness element size and spacing) are sufficient to determine the heat transfer. To this end, three SET samples, each with the same SET parameters, but with different physical arrangements of roughness are tested. The experimental approach follows that developed by Henry [7] - i.e. to measure

the heat transfer via non-invasive IR measurements of a heated flat plate.

Theoretical Analysis

In this section, the calculation of the convective heat transfer coefficient of airflow over a flat plate is discussed. The calculation of this coefficient requires a heat balance for a heated flat plate with airflow. Two types of convective heat transfer coefficients are presented: absolute and relative (to the un-perturbed flow).

Calculation of Convective Heat Transfer Coefficient

The convective heat transfer coefficient can be referenced to an appropriate value giving a relative coefficient. Henry developed a simple technique to calculate relative coefficients [7], in which the incoming heat flux $Q_{rad,in}$ is balanced by the sum of the heat flux losses, which are the convective flux Q_{conv}, the conduction flux Q_{cond}, and the radiation flux $Q_{rad,out}$:

$$Q_{rad,in} = Q_{conv} + Q_{cond} + Q_{rad,out}. \quad (1)$$

If the roughness element and the flat plate are made of a non-conducting material, the conduction flux is negligible. If surface temperatures are kept relatively close to ambient temperatures, the radiation flux is also negligible. Under these assumptions, the heat balance is dominated by the incoming radiation flux and the convection flux loss, defined as:

$$Q_{conv} = h(T_{surf} - T_\infty) \quad (2)$$

where h is the convective heat transfer coefficient, T_{surf} is the surface temperature and T_∞ is the free stream temperature. If the incoming heat flux is uniform over the surface, the convection flux is also uniform. Calling the plate upstream of the roughness element the unperturbed area and the roughness element the perturbed area, the following relation holds:

$$h_p(T_{surf,p} - T_\infty) = h_u(T_{surf,u} - T_\infty) \quad (3)$$

where the subscript u refers to unperturbed and p to perturbed (i.e. with roughness). The relative convective heat transfer coefficient can then defined in the following way:

$$\frac{h_p}{h_u} = \frac{(T_{surf,u} - T_\infty)}{(T_{surf,p} - T_\infty)}. \quad (4)$$

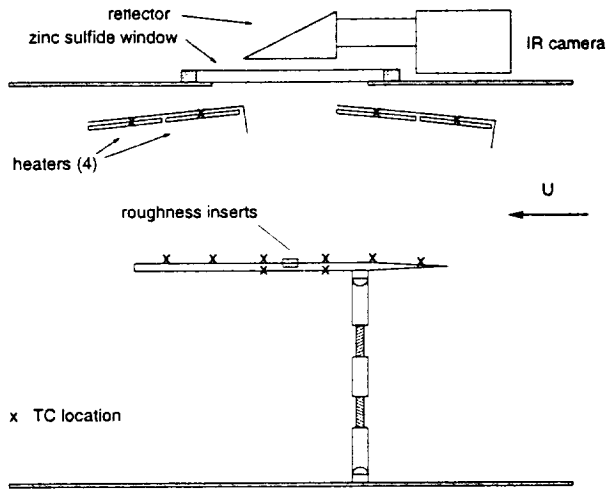

Figure 2: Schematic of Wind Tunnel test setup.

To calculate absolute convective heat transfer coefficients, all the terms in the heat balance equation 1, need to be known. However, as stated before, and experimentally confirmed, the outward radiation and through-plate conduction heat losses can be safely ignored. The incoming radiation flux, produced by IR heaters, is defined as:

$$Q_{rad,in} = F\sigma\epsilon_h(T_h^4 - T_{surf}^4) \quad (5)$$

where F is the view factor (a geometric factor associated with the placement of the IR heaters [8]), σ is the Stefan-Boltzmann constant, ϵ_h is the emissivity of the heaters and T_h is the temperature of the heaters. The view factor was computed for the geometry of the current experiment assuming uniform temperature distribution on the heaters. It can also be determined by a zero-flow measurement of temperature where the incoming radiation flux is balenced by conduction through the plate and by free convection from the surface [4].

Experimental Design and Procedure

Overall Setup

The experiment was conducted in a low velocity wind tunnel at NASA Lewis Research Center and the setup is shown schematically in Figure 2. The wind tunnel's test section measured 15.2cm wide by 68.6cm high (6" x 27") and its maximum velocity attainable was approximately 46 m/sec (103 mph). Clear tunnel turbulence levels were less than 0.5%. Four thermocouples located around the perimeter of the inlet of the tunnel measured the flow stagnation

temperature. The flat plate was 15.2cm wide, the width of the test section, 50.8cm long and 1.3cm thick (6"x20"x0.5"), and was made out of Plexiglas. The plate had a beveled leading edge, at an angle of 3°, and a 1.5mm nose diameter. The flat plate could be rotated to different angles of attack. Two roughness inserts were located 25.4cm (10") downstream from the leading edge at two spanwise locations. The plate was instrumented with a row of 12 pressure taps along its centerline. A pitot-static tube was placed upstream of the flat plate to measure free stream total and dynamic pressures.

The flat plate was heated by four IR ceramic heaters placed at the top of the test section and shielded from the flow by small fins. The temperature of each heater (measured by a thermocouple located at the center of each device) was controlled by varying the supply voltage with a Variac. The plate temperature was measured with an Inframetrics 600 IR camera located outside the wind tunnel and focused on the test plate through a Zinc Sulfide window. The camera had an accuracy of 1K, resolution of 0.05K, and operated at the wavelength range of 8-14 μm. The view area of the camera was approximately 12.7cm x 10.2cm (5"x4"). IR camera images were recorded on a VCR for later analysis. The images were calibrated by means of an array of 12 surface-mounted thermocouples embedded in the test plate at six streamwise locations. Lastly, four thermocouples were mounted on the lower surface of the plate, from which conductive losses could be estimated. Complete details of the experimental setup can be found in Torres [15].

Roughness elements

Figure 3 shows a schematic top-view of the location of the plugs in the plate and a detail of their insertion in the plate. The plugs were placed at two spanwise locations, spaced 5 cm (2") from center to center, giving a 3.6cm (1.4") spacing from the tunnel walls, assumed to be enough to avoid side wall effects on the flow over the roughness. The front view at the bottom of Figure 3 shows the three types of plugs used and how they were inserted in the plate. The plate was 1.3cm (1/2") thick and the plugs were 1cm (3/8") thick. In addition to the casting and roughness element pattern plugs, plain plugs were used for smooth flat plate heat transfer studies. When mounted, the plain plugs were flush with the surface. The roughness element pattern plugs were also flush with the surface, only exposing the roughness

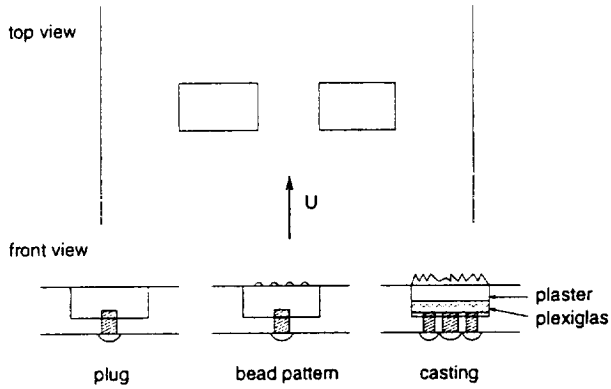

Figure 3: Schematic top view of the location of the plugs in the flat plate and front view detail of the plug insertion into the flat plate

elements to the flow. The height of the casting exposed to the flow was varied using the push-pull arrangement shown. The middle screw pulled on the plug and the two side screws pushed. Three heights were tested, varying 0.4mm from each other. The top surface of the flat plate and plugs were painted flat black to aid in the IR camera measurements.

The roughness samples used were the natural ice roughness castings (originally obtained by Masiulaniec et al.), and three SET-based simulated roughness patterns, provided by Orr. The castings were already suitable for a flat plate study in a "dry" wind tunnel. However, the original samples were cast in aluminum and so, to minimize conduction losses, the samples were re-cast in plaster. The roughness element patterns were produced employing SET on a photograph of the natural ice roughness casting. Using the parameters extracted from SET, the natural ice roughness was modeled by a pattern of roughness elements of 0.93mm diameter, spaced 1.79mm from each other. With these characteristics, three roughness element patterns were fabricated: a rectangular pattern, a staggered, or offset pattern, and a pseudo-random pattern, as shown in Figure 4. The bead density is approximately the same in all three patterns.

Experimental Procedure

The experimental procedure was as follows: First, the heaters were adjusted to achieve uniform heating on the plate without airflow. Once this condition was reached, the heater temperatures were recorded, the flow was turned on and the voltage on the heaters was increased until the same recorded temperatures

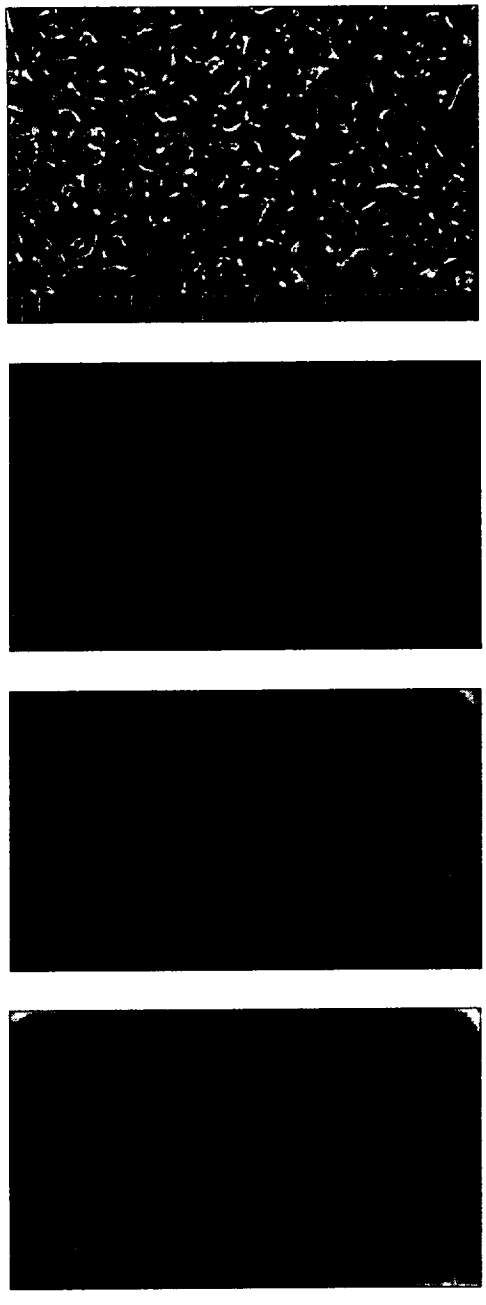

Figure 4: Photos of the original accretion casting, accompanied by three artificial roughness element patterns based on the SET analysis. Each plug is 17 mm × 28 mm.

were reached. In this manner, the convective cooling of the heaters due to the air flow was compensated and it was assumed that the radiation distribution reaching the plate was approximately the same as for the no airflow case. The thermograms were then calibrated using the surface thermocouples. The intensity of the thermogram at the thermocouple locations was measured. These intensity readings were converted to radiation level units and then plotted versus thermocouple temperature to produce a calibration curve.

Measurements were performed with the flat plate at two angles of attack, 0°and 20°. For the two different angles of attack, three types of tests were done. First, temperature distributions for a smooth flat plate were measured, then tests with the bead patterns and casting plugs were done. The casting and its three associated bead patterns were tested. The castings were tested at three different heights at 0 °angle of attack. No castings were tested at 20°angle of attack. At 0°angle of attack, the velocities tested were 27.0, 34.8, 42.5, and 46.4m/s. At 20°angle of attack, tests were run at 38.7 and 46.4m/s. Only part of the data is presented in this paper. A complete set of results may be found in Torres [15].

Results and Discussion

Smooth Flat Plate Convective Heat Transfer Coefficients

Convective heat transfer coefficients were calculated from the thermocouple data for the smooth flat plate and compared to theoretical results. These are shown in Figure 5 for both the 0°and 20°angles of attack at 35 m/s and are compared to the theoretical solutions for laminar and turbulent boundary layers. The values for the heat transfer coefficient at 0°do not match very well with the theoretical predictions and the higher value of h suggests that the boundary layer is already turbulent on the plate, a suspicion confirmed using a hot-wire to probe the state of the boundary layer. However, at 20°, the smooth plate coefficients do match well with the laminar solution. The differences are probably due to the acceleration of the core flow, not accounted for in the convective heat transfer coefficient solution. Pressure distribution data (not presented here) shows that the velocity of the flow is lower than U_∞ upstream of $x = 10$", and higher than U_∞ downstream. This acceleration explains coefficients lower than theoretical at $x = 5$", and higher coefficients at $x = 12$" and 15". Higher coefficients at $x = 2$" might be due to a region of recirculation upstream of the stagnation point.

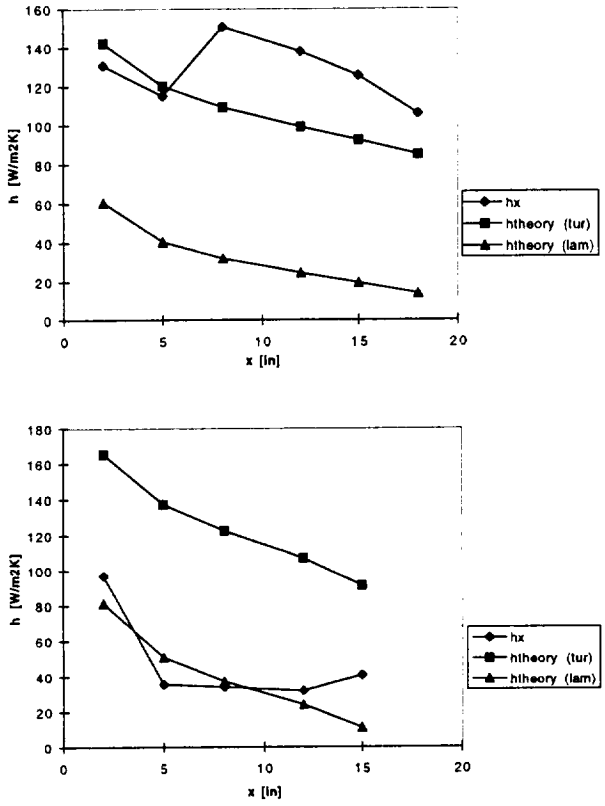

Figure 5: Experimental and theoretical convective heat transfer coefficients for the smooth plate at 0°and 20°angle of attack and 35 m/s (derived from thermocouple data).

Effect of Roughness on the Convective Heat Transfer Coefficient

Convective heat transfer coefficient profiles for the plate at 20°are shown in Figures 6 for the three artificial roughness inserts. These profiles are compared to the smooth plate results and the turbulent and laminar solutions. Upstream of the roughness, excellent agreement is observed between the profiles for the plate with roughness and the smooth plate. The convective coefficient transitions in all cases from its laminar boundary layer value to its turbulent boundary layer value, indicating that the roughness (at $x = 10$") is tripping the boundary layer. The rectangular and offset arrays show similar results, although the pseudo-random array is observed to become fully turbulent a little later, between $x = 12$" and $x = 15$". This delay in the transition location is consistent with the experiments of Bragg et al [2] who also found that large roughness elements lo-

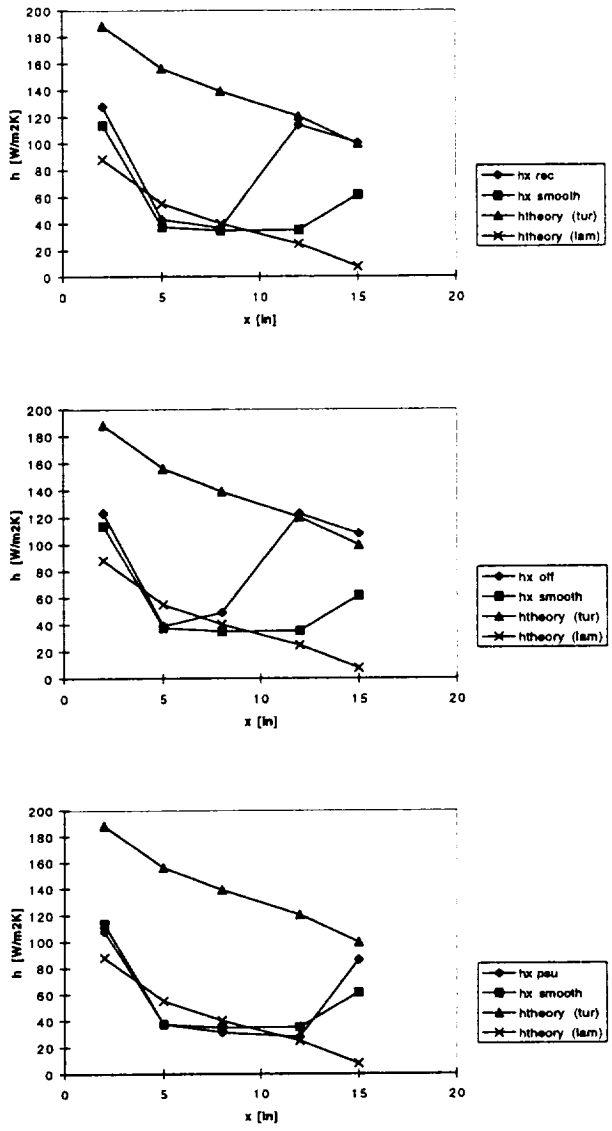

Figure 6: Experimental and theoretical convective heat transfer coefficients for the plate at 20°angle of attack with the rectangular, offset and pseudo-random roughness samples shown at the top, middle and bottom respectively. (computed from TC data).

cated in a faborable pressure gradient forced a gradual rather than immediate transition to turbulence.

A typical Infrared thermogram is shown in Figure 7. Darker regions indicate cooler temperatures and thus higher convective heat transfer. The opposite is true for lighter regions. Also note the wakes of cooler regions downstream of the plugs, a result also observed by Henry [7]. Some unevenness is also

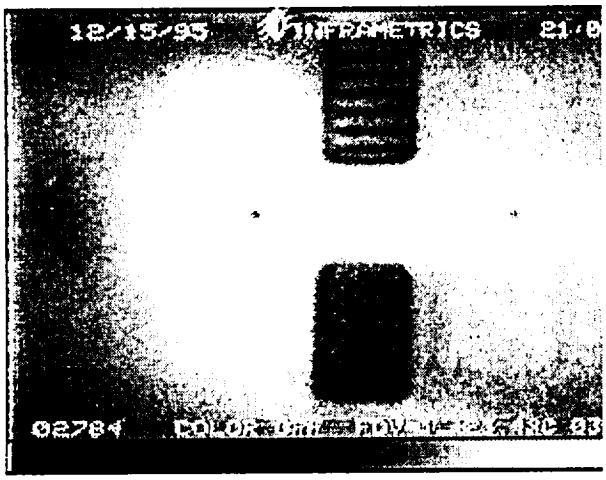

Figure 7: Typical thermogram of inserts 1 and 2, $\theta = 20°, U = 46$m/s. Flow is from left to right.

observed, for example, the bright spot at the center left of the inserts and the gaps between the plugs and the flat plate. These may be due to uneven heating from the ceramic heats, but are more likely due to nonuniform adsorption and reflection by the surface. In particular, the gaps around each plug were sealed with a filler that was not matched for thermal conductivity or emissivity to the surrounding plexiglass plate.

Figures 8, 9 and 10 shows the detailed thermogram convective heat transfer coefficient profile for the three artificial roughness samples (samples b, c and d in Figure 4). The raw IR image is shown at the top of each figure. From this image, two lines are extracted - one being the spanwise-averaged temperature over the roughness samples, the other being the temperature from a strip of undisturbed flow on the side of the roughness sample. From these temperature distributions, convective heat transfer coefficients are then computed (shown in the third frame). Lastly, the rough-surface heat transfer coefficient is divided by its undisturbed counterpart to give the ehanced heat transfer coefficient, plotted in the last frame. The stars on the temperature and heat transfer plots show data derived from thermocouples and generally agree quite well with the IR data. It is interesting to note that there are not observed to be strong wakes associated with the roughness elements. This is probably due to two factors - the strong pressure gradient as well as the relatively small size of the roughness elements compared to the boundary layer thickness.

Several features can be observed in the thermo-

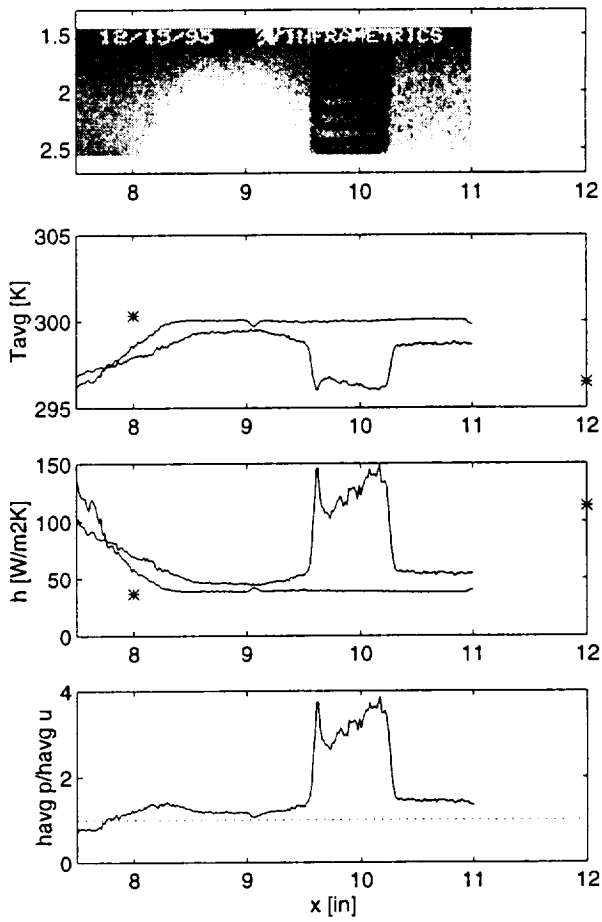

Figure 8: IR image, temperature, convective heat transfer coefficient and enhanced heat transfer coefficient for the rectangular roughness array (Figure 4 (b). $U_\infty = 46$m/s, θ =20°.

gram data. Firstly, the heat transfer is enhanced, as expected by the roughness elements, although the exact placement of the beads does appear to have a strong effect on the enhanced transfer. However, one must be careful, if one compares the rectangular and offset arrays (Figures 9 and 10), one observes that the leading and trailing edges of the image result in sharp spikes which, on examination of the images, is clearly associated with the filler around the plug and not the roughness elements. Discarding the spikes in h associated with this feature, the heat transfer coefficient is roughly comparable, reaching about 3.5 times the undisturbed value. However, the trend of the two arrays is different, with the rectangular array showong a monotonic increase with streamwise distance, x, while the offset is more uniform over the length of the array. The pseudo-random array does

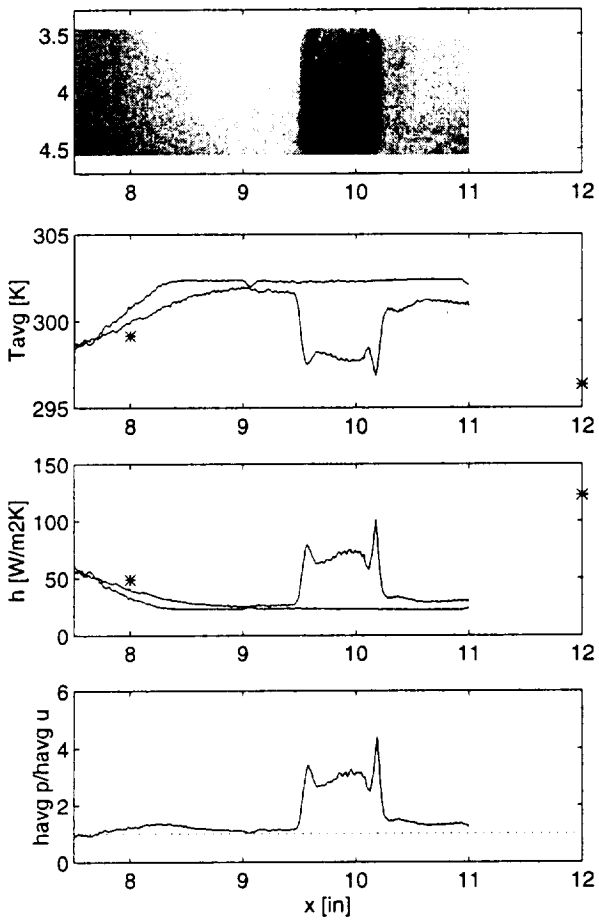

Figure 9: IR image, temperature, convective heat transfer coefficient and enhanced heat transfer coefficient for the offset roughness array (Figure 4 (*c*). U_∞ = 46m/s, θ =20°.

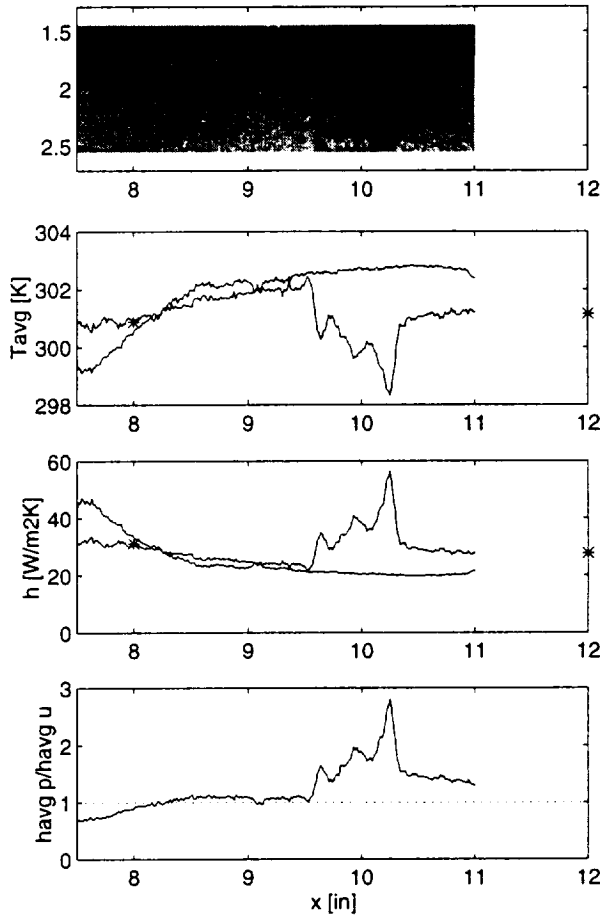

Figure 10: IR image, temperature, convective heat transfer coefficient and enhanced heat transfer coefficient for the pseudo-random roughness array (Figure 4 (*d*). U_∞ = 46m/s, θ =20°.

show a more marked difference. Like the rectangular array, the heat transfer enhancement appears to increase monotonically over the length of the insert. However, for this case, the peak enhancement only reaches about 2.5 times its undisturbed value.

By integrating the heat transfer enhacement over the streamwise direction, an average enhacement can be obtained and thus the overall effects of all three arrays can be compared. This is shown in Figure 11, which also shows results for a lower speed, U_∞ = 39, and the qualitative results of the previous figures are reproduced. Specifically that the rectangular and offset arrays show little difference, while the pseudo-random array exibits a lower heat transfer enhacement than the orderly-spaced roughness inserts.

Validation of SET Roughness Modeling

Although there was an opportunity to do direct comparisons between the castings and their associated SET roughness patterns, the resultant data is somewhat sparse (the casting data is only available for the 0°angle of attack) and is inconclusive. The enhanced heat transfer coefficients of the direct castings (not shown here) are significantly higher that those observed with the artificial roughness, but can be ascribed to two factors. Firstly, the amplitude (height) of the castings was signficantly larger than the height of the artificial roughness, so direct comparisons cannot be made. The difference in height is crucial as the relative size of the roughness elements with respect to the boundary layer (k/δ) is a key determining paramter. Secondly, as mentioned earlier,

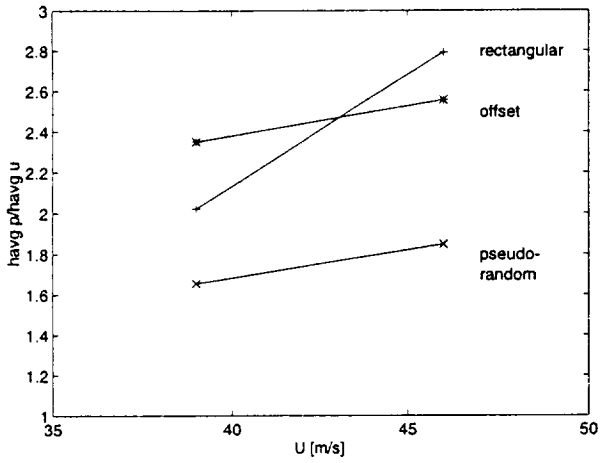

Figure 11: Average convective heat transfer enhancement for SET arrays, $\theta = 20°$.

the castings are strictly not appropriate for analysis by the SET method, which is better suited to early accretions typified by isolated roughness elements. Nevertheless, we can make some observations based on the current results which can help improve SET as a roughness modeling technique.

- As observed in the thermogram data presented here, although they are not strongly visible, the wakes of heat transfer enhancement produced by single roughness elements contribute to the average enhancement of the roughness element array (as evidenced by the differences between the rectangular and offset arrays). The interaction between wakes and roughness elements is also important. Thus, the roughness spacing in the flow and in the span direction are important and more work should be done in characterizing this better.

- Currently, the SET does not include any data on the height of the roughness elements. This is due to the fact that the original video data [6] contained no information regarding the height. However, if these data are available, the SET can include it without any generic difficulties. The importance of the height of the roughness (with respect to the local boundary layer thickness) is clearly paramount to the scheme's success.

Concluding Remarks

The primary objective of this study was to demonstrate a coherent and unified approach to the determination of roughness-assisted heat transfer associated with early roughness in ice accretions. That goal required that we provide four milestones: (a) Obtain high quality closeup video data of early ice accertions, (b) develop a characterization scheme to reduce observed roughness to a few descriptive parameters that effectively capture the roughness' role in enhancing heat transfer during an accretion; (c) re-create simulated roughness, using these descripting parameters and finally (d) measure the heat transfer associated with the simulated roughness. Once all these pieces are in place, the measured heat transfer coefficient can be used in modeling codes such as LEWICE, and the prediced accretion can be compared with the observed accretion that initiated the entire process.

Parts (a) - (c) have been provided in work prior to that presented here [6, 11, 12] and the basis for non-invasive measurement was provided by Henry et al [7]. The contribution of the current paper, then, is to complete the final step, (d) and to provide the measurements of the enhanced heat transfer coefficients. This has been achieved and the overall scheme is thus believed to be feasible for more general predictions of accretion-enhanced heat transfer. In addition, the IR mapping of the absolute heat transfer coefficient is demonstrated here to be a powerful technique that deserves further development. It could quite easily be extended to more complex geometries and unsteady measurements all of which would prove very useful in understanding heat transfer in geometrically complex systems such as those observed in early ice accretions.

Having said that, however, we must recognize that the present results are only the first step in this process. Although the general technique for this kind of experiment has been demonstrated, the absolute quality of the data presented in this paper is uneven and should be regarded as a proof of concept. Several problems were identified which should be fixed in subsequent experimental efforts. These include:

1. Ideally, the heaters should be placed completely out of the flow path so that they are not cooled by the freestream flow. This cooling required the adjustment of the heater voltages to match surface temperatures on the assumption that (a) the surface temperature was uniform over

the entire heater and (b) that equivalent surface temperatures implies equivalent radiation to the plate. The first of these assumptions, in particular, is suspect. Mounting the heaters out of the flow path would enable control of the incoming radiation flux independently of the free stream velocity.

2. The flow quality obtained in the facility left much to be desired. Leading edge separation was observed and should be fixed with a trailing edge flap to control the attachment point. The blockage of the heaters should be reduced (by moving them outside the tunnel), the gaps between the inserts and the plate should be minimized and treated properly so that they do not give false readings to the IR camera. Lastly, more complete boundary layer data should be taken to determine the displacement and momentum thicknesses more accurately. This last piece of data would greatly aid in the comparisons with theoretical heat transfer coefficients.

3. The IR measurements could be improved by shielding the camera better from stray reflectons and by better matching the emisivities of the materials used in the experiment. More uniform heating might also be obtained by using larger arrays of smaller ceramic heaters.

4. Many more roughness samples need to be tested, both from the same icing images and from many more icing images derived from different cloud conditions and accretion characteristics. The samples here show some variations which indicate that the SET parameters chosen (size and separation) may not be complete or optimal. However, more testing under different conditions (roughness height, boundary layer thickness, choices of spacing, etc) needs to be conducted to establish what are the true limitations of the SET descriptions and what data collapses well.

This work was supported by NASA Lewis, monitored by Dr. M. Potapczuk.

References

[1] M. Bragg, M. Kerho and M. Cummings. "Effect of Initial Ice Roughness on Airfoil Aerodynamics", AIAA 94-0800, January 1994.

[2] M. Bragg, M. Kerho and M. Cummings. "Airfoil Boundary Layer due to Large Leading-edge Roughness", AIAA 95-0536, January 1995.

[3] M. Bragg. "Airfoil Boundary Layer due to Large Leading-edge Roughness", Icing Roughness Working Group Meeting, NASA Lewis Research Center, July 26, 1995.

[4] L. C. Burmeister, *Convective Heat Transfer*, John Wiley, New York, NY, Second Edition, 1993.

[5] N. Dukhan, G. J. Van Fossen, Jr., K. C. Masiulaniec, and K. J. DeWitt, "Convective Heat Transfer from Castings of Ice Roughened Surfaces in Horizontal Flight", International Icing Symposium, September 1995.

[6] R. J. Hansman Jr., K. S. Breuer, D. Hazan, A. Reehorst, and M. Vargas. "Close-up Analysis of Aircraft Ice Accretion", AIAA 93-0029, January 1993.

[7] R. C. Henry, K. S. Breuer, and R. J. Hansman Jr. "Heat Transfer Variation on Protuberances and Surface Roughness Elements", *Journal of Thermophysics and Heat Transfer*, Vol. 9, No. 1, January-March 1995.

[8] F. P. Incropera, and D. P. DeWitt, *Introduction to Heat Transfer*, John Wiley, New York, NY, Second Edition, 1990.

[9] W. M. Kays, and M. E. Crawford, *Convective Heat and Mass Transfer*, McGraw-Hill, New York, NY, Second Edition, 1980.

[10] K. C. Masiulaniec, K. J. DeWitt, N. Dukhan, and G. J. Van Fossen, Jr. "Experimental Technique and Assessment for Measuring the Convective Heat Transfer from Natural Ice Accretions", AIAA 95-0537, January 1995.

[11] D.J. Orr, K. S. Breuer, and R. J. Hansman, Jr. "Quantitative Analysis of Ice Accretion Roughness Using Spectral and Stochastic Techniques", AIAA 95-0888, January 1995.

[12] D.J. Orr, K. S. Breuer, B. E. Torres and R. J. Hansman, Jr. "Spectral Analysis and Experimental Modeling of Ice Accretion Roughness", AIAA 96-0865, January 1996.

[13] A. R. Porro, T. G. Keith, Jr., W. R. Hingst, R. M. Chriss, and K. D. Seablom, "Development of a Laser-Induced Heat Flux Technique for Measurement of Convective Heat Transfer

Coefficients in a Supersonic Flowfield", NASA TM 103778, March 1991.

[14] J. Shin, "Characteristics of Surface Roughness Associated with Leading Edge Ice Accretion", AIAA 94-0799, January 1994.

[15] B. E. Torres "Heat Transfer Measurements of Surfaces with Natural and Simulated Ice Accrection Roughness", M.S. Thesis, Department of Aeronautics and Astronautics, M.I.T. September1996.

[16] F. M. White, *Viscous Fluid Flow*, McGraw-Hil, New York, NY, 1974.